

## Photocatalytic degradation studies of malachite green dye by hydrothermally synthesized Cobalt Vanadate nanoparticles

Lakshmana Naik Ramavathu<sup>1,\*</sup>, Bala Narsaiah Tumma<sup>2</sup>, Ponniah Justin<sup>3</sup>

<sup>1</sup> Department of Chemical Engineering, Rajiv Gandhi University of Knowledge Technologies, RK Valley, Kadapa-516330, India

<sup>2</sup> Department of Chemical Engineering, JNTUACEA, Ananthapuramu-515002, India

<sup>3</sup> Department of Chemistry, Rajiv Gandhi University of Knowledge Technologies, RK Valley, Kadapa-516330, India

Received 16 August 2022,

revised 23 September 2022,

accepted 01 October 2022,

available 03 October 2022

### Abstract

Cobalt vanadate ( $\text{Co}_3\text{V}_2\text{O}_8$ ) nanoparticles were prepared by a hydrothermal process using ammonia metavanadate and cobalt nitrate as precursors and calcined at 450 °C to obtain pure  $\text{Co}_3\text{V}_2\text{O}_8$  nanoparticles. The sample was characterized by scanning electron microscopy, X-ray diffraction, Fourier transform infrared, and UV-visible diffuse reflectance spectroscopy. The characterization analysis confirmed variations in the structure, shape, functional group, and energy gap of  $\text{Co}_3\text{V}_2\text{O}_8$  nanoparticles. Using the Tauc relationship, the energy band gap was determined by analyzing the Tauc curve. The nanoparticles obtained had an average size of 40 nm and found the zeta potential of the nanoparticles was -78 mV, indicating good dispersion and stability. The photocatalytic activity of  $\text{Co}_3\text{V}_2\text{O}_8$  nanoparticles through the degradation of malachite green dye was investigated under UV light irradiation. According to the results,  $\text{Co}_3\text{V}_2\text{O}_8$  nanoparticles showed a maximum removal efficiency of 89 percent in 60 minutes. It shows that synthesized  $\text{Co}_3\text{V}_2\text{O}_8$  nanoparticles have a strong potential for application as a photocatalyst to degrade textile dyes in wastewater treatment rapidly.

**Keywords:** Cobalt Vanadate; Degradation; Hydrothermal Synthesis; Malachite Green; Photocatalyst; Wastewater Treatment.

### How to cite this article

Naik Ramavathu L., Narsaiah Tumma B., Justin P. Photocatalytic degradation studies of malachite green dye by hydrothermally synthesized Cobalt Vanadate nanoparticles. *Int. J. Nano Dimens.*, 2023; 14(2): 145-156.

## INTRODUCTION

Non-biodegradable contaminants in the aquatic system have become increasingly serious and severe recently due to rapid industrial and socio-economic development and significantly impacts on human and animal health [1]. Dyes from manufacturing industries such as pharmaceutical, leather, paper, textile, food, printing, cosmetics and rubber also belong to this group. They pose a significant threat to public health and the environmental protection. These are all dangerous and can cause serious health problems to live beings. Malachite Green (M.G.) is the most hazardous synthetic dye used in industrial and scientific applications [2]. Due

to its easy interaction with membranes, M.G. can penetrate cells [3]. It is used in various fields as a food colouring and colouring additive [4, 5]. Therefore, it is highly recommended to convert the colours into safe shapes.

For photocatalytic applications, scientists have searched for a suitable material with excellent exponential stability and exciting properties [6-9]. The stability and versatility of transition metal oxides are best known in fields such as batteries [10], sensors [11], antimicrobial research [12], electronic devices [13], photocatalytic activity [14], etc. Because of these intriguing properties, scientists have experimented with a variety of mixed metal oxides to improve the performance of the nanomaterials [15]. Previous research

\* Corresponding Author Email: [lakshman2027@gmail.com](mailto:lakshman2027@gmail.com)



has shown that combining metal oxides such as  $\text{TiO}_2\text{-V}_2\text{O}_5$ ,  $\text{Co}_3\text{O}_4/\text{TiO}_2$ ,  $\text{WO}_3/\text{SnO}_2$ ,  $\text{CuO-NiO}$ , and others improves their performance efficiency in various sectors [16–19]. In this context, a cobalt and vanadium oxide combination has been investigated. Vanadium oxide is an n-type semiconductor and one of the most stable forms of  $\text{V}_2\text{O}_5$ , and cobalt oxide is a p-type transition metal with a wide variety of uses.  $\text{Co}_3\text{V}_2\text{O}_8$ , combined with other materials, can potentially be very effective in application. Numerous research groups have used metal vanadates (Zn, Co, Cu, Fe, Mn, Ni, etc.) as photocatalysts in recent years, and significant efforts have been made to synthesize various types of nanocomposite materials as mixed metal vanadates. Among the various trimetallic vanadates, cobalt vanadate has attracted particular interest due to its low cost, environmental friendliness, and availability. Due to their exceptional electrical properties, one-dimensional (1D) materials such as nanowires, nanorods, nanotubes, etc., are gaining importance, especially in energy-related applications [20]. They have a high surface area to volume ratio, which makes them suitable for technological applications.

Many biological, chemical, and physical techniques have been used to remove wastewater dyes and other hazardous contaminants. Although membrane coagulation, filtration, precipitation, flocculation, adsorption, and ion exchange techniques are commonly used for contaminant removal, they are not ideal for obliterating the contaminants [21-23]. Heterogeneous photocatalysis with semiconductor oxides has been used to complete the processing of organic pollutants into  $\text{CO}_2$ ,  $\text{H}_2\text{O}$  and inorganic salts [24]. Due to solar energy, photocatalysis in water treatment has an excellent position compared to other conventional approaches [25]. Nanomaterials have unique physical and chemical properties, such as increased surface area and defects on the surface. It would also be used in photocatalytic reactions. The optical properties of nanomaterials are mainly determined by their size and shape [26, 27]. Cobalt oxides are used in lithium-ion batteries, gas sensors, ceramics, heterogeneous catalysts, energy storage and other applications [28, 29]. Changing the size, distribution, and shape of nanoparticles makes heterogeneous catalysts more effective. Numerous methods are reported for synthesizing

cobalt vanadate nanocomposite, including coprecipitation, sol-gel in combination with thermal decomposition, green hydrothermal synthesis, pulsed laser deposition and solution combustion [30-32]. The hydrothermal approach has attracted significant interest as it allows fully controlled dispersion, size and shape of nanoparticles [33].

The present work reports on the synthesis of cobalt vanadate ( $\text{Co}_3\text{V}_2\text{O}_8$ ) nanocomposite by hydrothermal method. Using state-of-the-art analytical techniques, the  $\text{Co}_3\text{V}_2\text{O}_8$  produced was analyzed for crystallinity, phase, structural and morphological features. A photoreactor performed a thorough study of the synthesized materials' photocatalytic properties. This work aims to advance cleaner, more sustainable and environmentally friendly technologies for a better world by utilizing  $\text{Co}_3\text{V}_2\text{O}_8$ -based photocatalytic research for a wide range of energy applications.

## MATERIALS AND METHODS

### Materials

Materials used to prepare  $\text{Co}_3\text{V}_2\text{O}_8$  were of analytical reagent (A.R.) grade ( $\geq 99.0\%$  (RT)) purchased from Sigma Aldrich. They Cobalt (II) nitrate hexahydrate ( $\text{Co}(\text{NO}_3)_2 \cdot 6\text{H}_2\text{O}$ ), N-methyl-2-pyrrolidone ( $\text{C}_5\text{H}_9\text{NO}$ ), Ammonium metavanadate ( $\text{NH}_4\text{VO}_3$ ,  $\geq 99.0\%$ ), ethanol ( $\text{C}_2\text{H}_5\text{OH}$ ), urea ( $\text{CH}_4\text{N}_2\text{O}$ ), and double distilled water made in a laboratory.

### Synthesis of Cobalt Vanadate nanoparticles

A simple hydrothermal process was used to prepare the  $\text{Co}_3\text{V}_2\text{O}_8$  nanomaterial as shown in Fig. 1 (a-f). In a typical synthesis, 87.5 mL of N-Methyl-2-Pyrrolidone was added to a solution containing 1.323 g of  $\text{NH}_4\text{VO}_3$  (ammonium metavanadate) with steady magnetic stirring of 300 rpm for one hour. Further, 8.45 g of urea was added to the solution with steady stirring. Separately, 4.938 g of Cobalt (II) nitrate hexahydrate were added to 250 mL of water. Then, with continuous stirring, the above solutions were gently mixed. Finally, the blended solution was diluted to 350 mL, transferred to a Teflon-lined autoclave, and heat-treated for 36 hours at 180 °C. The powder in the autoclave was centrifuged, rinsed with deionized water, washed again with ethanol, and dried at 80 °C for 12 hours after cooling to room temperature. To generate highly crystalline powders, the dry material was calcined in air for 3 hours at 450 °C at a heating rate of 2 °C/min. The calcined sample

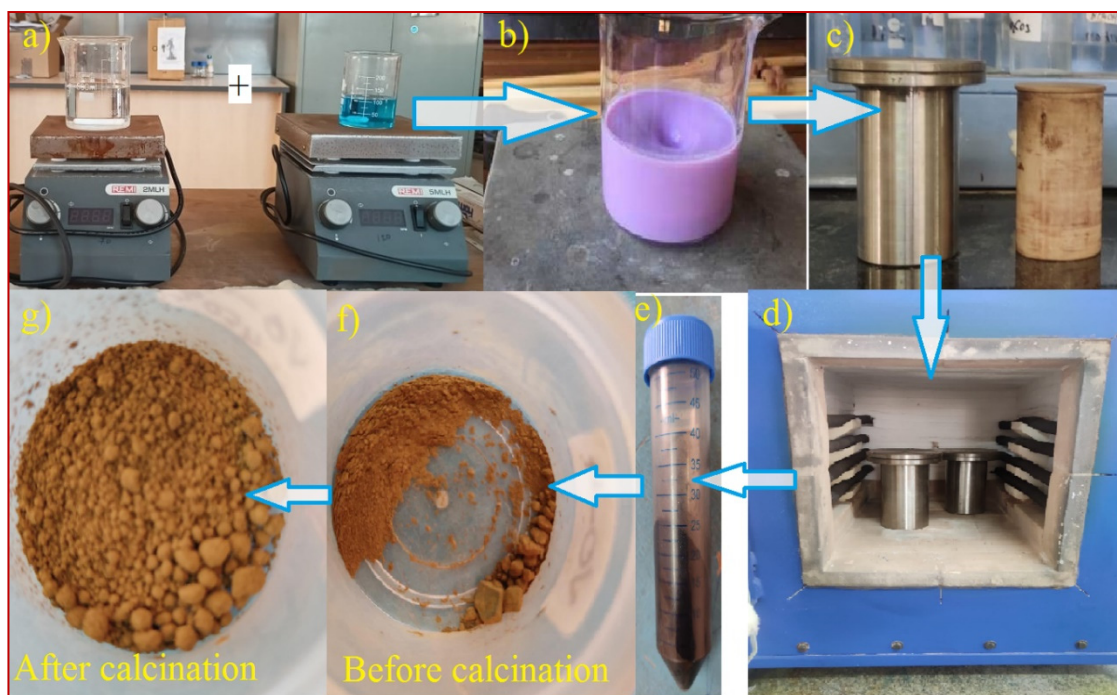


Fig 1. The schematic representation of synthesis of Cobalt vanadate (a) vanadium and cobalt precursor solutions (b) Solution obtained after stirring (c) Autoclaves (d) Heating (e) Centrifugation (f) Powder obtained after hydrothermal treatment (g) Powder obtained after calcination at 450 °C.

Table. 1. Lattice parameters of  $\text{Co}_3\text{V}_2\text{O}_8$  nanostructure.

Lattice parameters								
a (Å)	b (Å)	c (Å)	$\alpha = \beta = \gamma$	a/b	b/c	c/a	V (Å <sup>3</sup> )	D (nm) For plane (220)
6.03	11.486	8.312	90°	0.524	1.381	1.378	575.69	26.6
Space group: Cmca								
Structure: Orthorhombic								

shown in figure 1(g) is then used for further analysis.

#### Sample characterization

A diffractometer (CoK, PANalytical, X'Pert, data converted to CuK) was used to record X-ray powder diffraction (XRD) patterns. A JEOL2010 transmission electron microscopy was used to take the images. To analyze the characteristics of synthesized nanoparticles, UV–Visible absorption spectra were recorded using a UV 1800 spectrophotometer. A spectrometer was used to examine functional groups of the prepared sample using a Fourier transform infrared spectrometer (FT-IR) within the range of 4000 to 400  $\text{cm}^{-1}$  using the KBr pellet technique.

#### RESULTS AND DISCUSSION

Fig. 2, represents the XRD pattern of prepared nanoparticles, which show a sequence of distinctive characteristic peaks situated at  $2\theta$ : 19.74 (111), 29.6 (200), 33.54 (220), 43.48 (240), 58.06 (115), 63.21 (244) of synthesized cobalt vanadate nanoparticles. The quantitative analysis was performed using the HighScore Plus software bundle, v 3.0. These planes match well with JCPDS file no. 16-0675 [34] with Cmca space group and orthorhombic crystal system and other lattice parameters are shown in table.1. The crystalline size (D) of  $\text{Co}_3\text{V}_2\text{O}_8$  was calculated using the Debye-Scherrer's equation, which is shown below, and the spectra indicate strong peaks with a higher degree of crystallinity [35]:

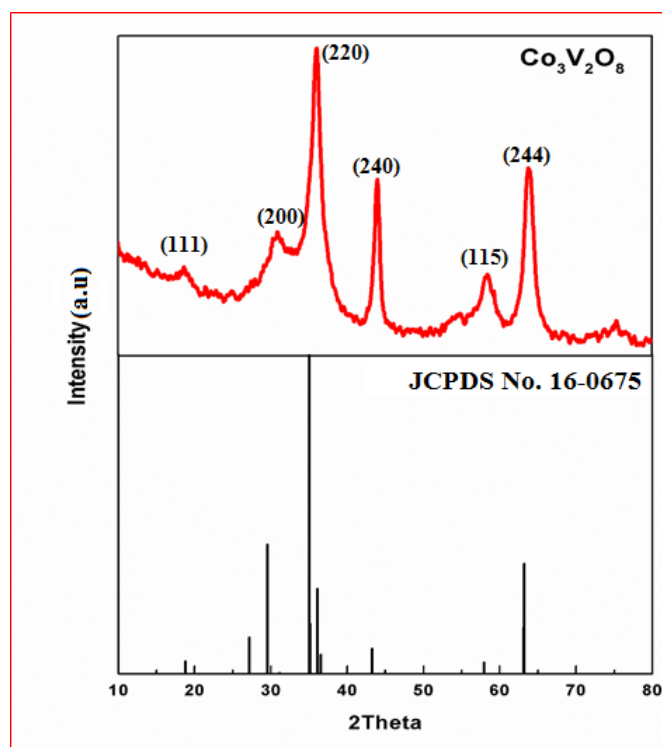


Fig. 2. XRD pattern of Cobalt Vanadate nanoparticles.

$$D = \frac{k\lambda}{\beta \cos\theta} \quad (1)$$

The average crystallite size of synthesized nanoparticles was deduced to be  $\sim 28.36$  nm.  $D$  is the average crystallite size,  $k$  is Scherrer's constant for orthorhombic structure (0.89),  $\theta$  is the Bragg's diffraction angle,  $\lambda$  is the wavelength (1.540 Å) of the X-ray source, and  $\beta$  is full width at half maximum (FWHM).

The morphology of hydrothermal prepared  $\text{Co}_3\text{V}_2\text{O}_8$  nanoparticles was examined using TEM images. The shape and sizes of  $\text{Co}_3\text{V}_2\text{O}_8$  nanoparticles are shown in Fig. 3. For calcination temperature, irregular morphologies of  $\text{Co}_3\text{V}_2\text{O}_8$  nanoparticles with minimal agglomeration were obtained. The particles were spherical primarily; however, at calcination temperature, more irregular morphologies of  $\text{Co}_3\text{V}_2\text{O}_8$  nanoparticles were noticed. This could be due to small primary particles aggregating to generate secondary or even ternary particles. The images of the hydrothermal nanomaterial formed in Fig. 3(a-b) show the material's circular and ovular structures nanospheres, with sizes ranging from 10 nm to 20

nm. Individual rock-like structures are piled-up agglomerations of smaller units, which may be explained by the solvent used. It displays many crystal planes as shown in Fig. 3 (c-d), proving the development of the crystalline structure. The TEM images demonstrate that the diameters of the nanoparticles were very near to the average crystallite ( $D_{\text{XRD}}$ ), indicating that the calcined synthesised nanoparticles did not combine into bigger crystallites.

Results of the FT-IR analysis are presented in Fig. 4. The broad absorption band centred in the range of  $3600\text{-}3000\text{ cm}^{-1}$  was due to  $\text{-O.H}$  [36, 37] and stretching vibrations of absorbed moisture available in the sample, as shown in the inset of Fig. 4. Vanadium stretching modes (V-O) are allocated to bands at wavenumber  $932\text{ cm}^{-1}$ , and V-O-V stretching was allocated to bands at  $775\text{ cm}^{-1}$ . The band has been investigated in the FTIR at  $430\text{ cm}^{-1}$  and is associated with the extended mode of CO-O-V and Co-O-Co inorganic bonds. As seen in all spectra, the strong peaks at wavenumber around  $572\text{ cm}^{-1}$  are characteristic of Co-O and O-Co-O stretching vibration, respectively.

The optical properties of  $\text{Co}_3\text{V}_2\text{O}_8$  nanoparticles were studied by measuring the ultraviolet-visible

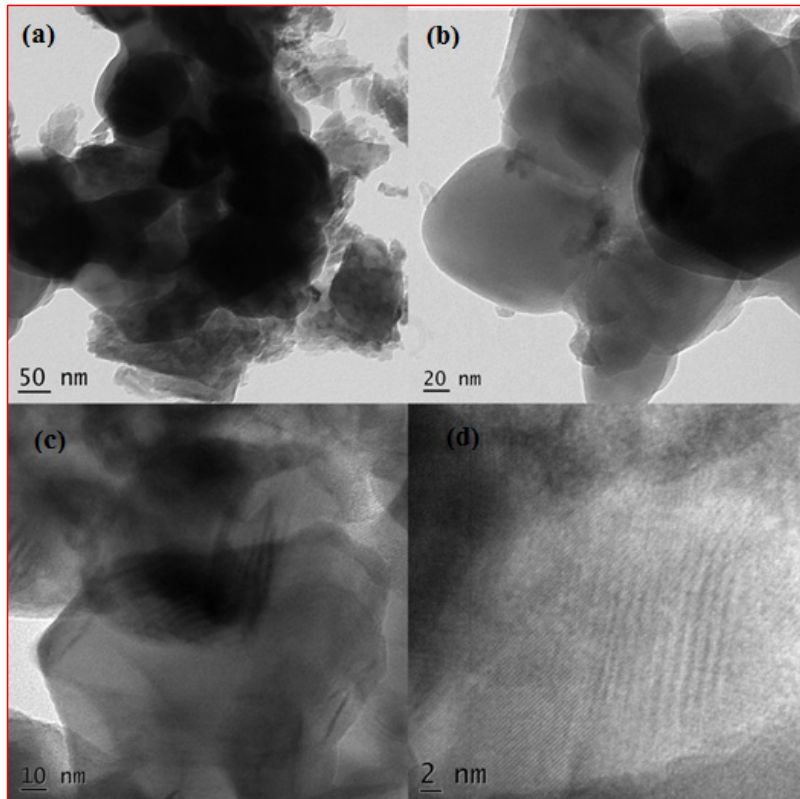


Fig. 3. Cobalt Vanadate TEM images (a-d) at different magnifications.

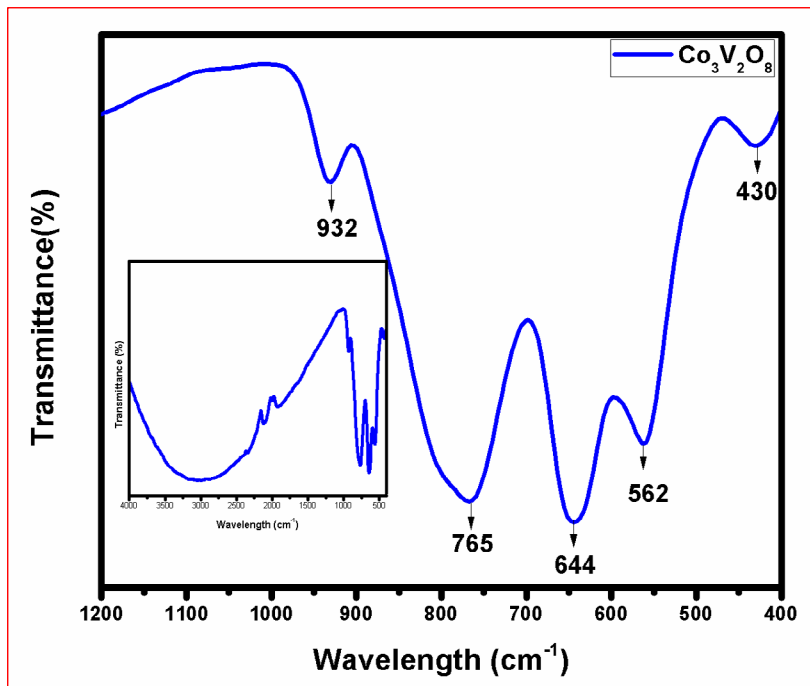


Fig. 4. FTIR spectroscopy of  $\text{Co}_3\text{V}_2\text{O}_8$ .

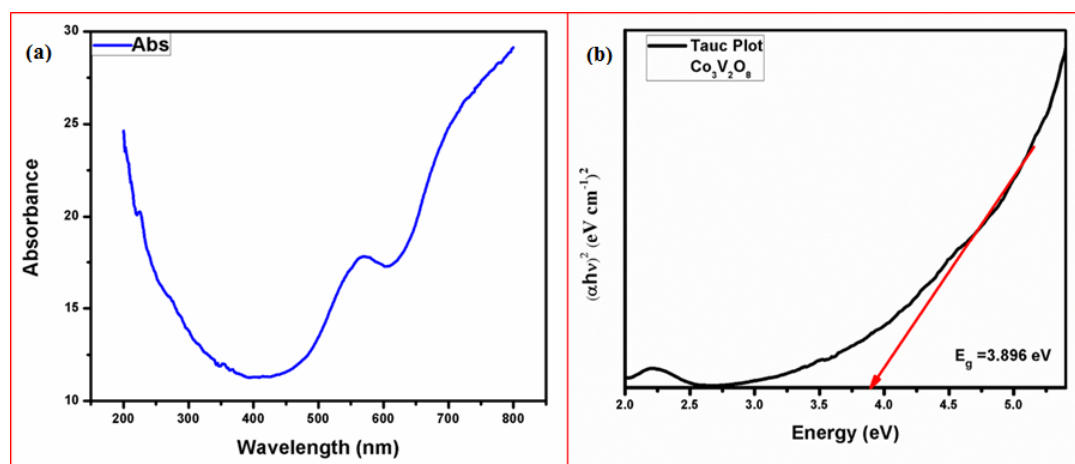


Fig. 5. (a) UV-Visible diffuse reflectance spectra (b) Tauc plot of  $(\alpha hv)^2$  Vs photon energy  $(hv)$ .

Table 2. Calculation Results of DLS.

Peak No	S.P Area Ratio	Mean	S.D.	Mode
1	1.00	45.5 nm	6.9 nm	42.8 nm
2	---	---	---	---
3	---	---	---	---
<b>Total</b>	<b>1.00</b>	<b>45.5 nm</b>	<b>6.9 nm</b>	<b>42.8 nm</b>
<b>Cumulant Operations</b>				
Z-Average : 40.0 nm				
PI : 3.334				

spectrum from 200 nm to 800 nm, as shown in Fig. 5(a). The synthetic composite has a broad spectrum band ranging from ultraviolet to visible light, reflects a broad spectrum of absorbed light by  $\text{Co}_3\text{V}_2\text{O}_8$  nanoparticles, and improves optical properties. This has been explained as a result of the characteristic intrinsic bandgap absorption of cobalt oxides caused by the photoexcitation of electrons from their valence bands to the conducting bands. To study the band gap energy of nanocomposite particles, the Tauc diagram [38] was plotted using equation (2), as shown in Fig. 5(b) and the band gap energy was estimated by drawing its tangent line:

$$(\alpha hv)^2 = A(hv - E_g) \quad (2)$$

Where  $\alpha$ ,  $h$ ,  $v$  and  $A$  are absorption coefficients, Planck constant, frequency and absorption, respectively. Fig. 5 shows the nanoparticle's calculated band gap energy, which was found to be 3.896 eV [39]. Several properties, such

as crystallite size, specific surface area, defect locations, etc. can all affect band gap energy

The size and the distribution of the  $\text{Co}_3\text{V}_2\text{O}_8$  particles were further verified by the dynamic light scattering (DLS) particle size analyzer, as shown in table 2 and Fig. 6. Particle size analysis shows that the range of  $\text{Co}_3\text{V}_2\text{O}_8$  nanoparticles had a size of 35–60 nm with a mean particle size of 42.8 nm [40]. The polydispersity index (P.I.) of nanoparticles was found to be 3.334. Dynamic light scattering analysis was used to measure the zeta potential value of synthesized  $\text{Co}_3\text{V}_2\text{O}_8$  nanoparticles. The zeta potential of the synthesized  $\text{Co}_3\text{V}_2\text{O}_8$  is essential in determining its shelf life. The zeta potential of  $\text{Co}_3\text{V}_2\text{O}_8$  was found to be -48.8 mV in this study, as shown in Fig. 7. Due to negative-negative repulsion, high negative zeta potential indicates that  $\text{Co}_3\text{V}_2\text{O}_8$  is long-term stable without agglomeration and promotes strong colloidal nature, high scatter of  $\text{Co}_3\text{V}_2\text{O}_8$  produced [41]. High stability is required to use nanomaterials in photo catalysts and energy storage devices.

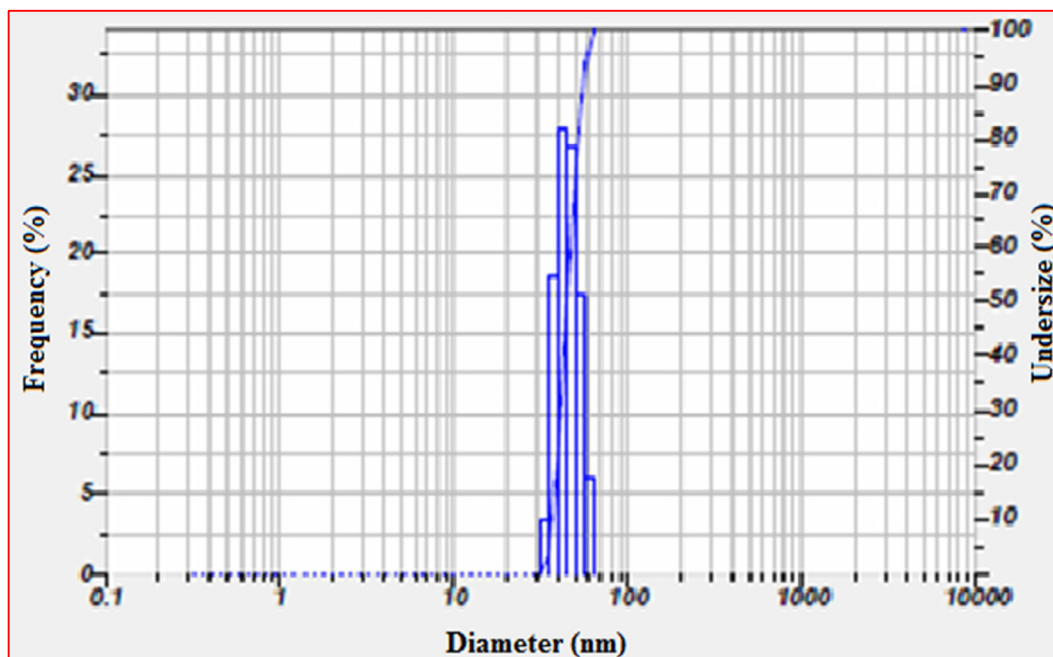


Fig. 6. Analysis of average particle size, particle size distribution and polydispersity index of  $\text{Co}_3\text{V}_2\text{O}_8$ .

#### Photocatalytic studies of $\text{Co}_3\text{V}_2\text{O}_8$

The photocatalytic reactor comprises a 125 W mercury vapour lamp that serves as an ultraviolet light source. A pollutant solution containing 20 parts per million (ppm) of 250 mL was poured into the circular glass reactor, adding 60 mg of the catalyst. The distance between the UV Source and pollutant solution was 21 cm. An open environment was chosen for all the photocatalytic experiments.

The industrial dyes, namely malachite green (M.G.) degradation studies of the synthesized  $\text{Co}_3\text{V}_2\text{O}_8$  photocatalyst, were examined under irradiation with ultraviolet light at regular intervals (15 min) up to 60 min. The first degradation performance was observed under dark conditions by scanning the 20ppm dye solution separately, and it was found that the dye solution underwent no appreciable change. Next, degradation studies were performed under the UV light for some time as an initial confirmatory test and noticeable deterioration of the dye solution was observed. Finally, dye degradation studies were performed considering time as a parameter under UV. Light exposure by taking  $\text{Co}_3\text{V}_2\text{O}_8$  as a catalyst for the dye at room temperature.

Based on these findings, photocatalytic tests for the degradation of M.G. Dyeing were carried

out in the presence of a catalyst for 60 minutes. M.G. has absorption peaks at 592 nm, as shown in Fig. 8(a) [42, 43]. When the dye solution is exposed to UV light, the decolorization clearly distinguishes photocatalytic observation from photolysis. The photocatalytic degradation analysis was carried out for M.G. using the synthesized catalyst after preparing a dye solution containing 20 ppm. Each solution included 60 mg of the Photocatalyst ( $\text{Co}_3\text{V}_2\text{O}_8$ ), individually mixed with the M.G. dye solution. The degradation efficiency of the dyes was determined under UV irradiation and at 15-minute intervals by subjecting a known amount of solution to the UV-Vis Spectrometer; the resulting UV-Vis spectra of the dyes are depicted in Fig. 8 (a) (M.G. dye). There was a frequent drop in the dye's absorption band; as a result, the degradation increased with time.

The absorption peaks gradually decrease with irradiation time when the solution is irradiated with ultraviolet (UV) light in the presence of the catalyst, confirming the enhanced photocatalytic activity of  $\text{Co}_3\text{V}_2\text{O}_8$  nanomaterial. The reduction in absorption peak for M.G. occurred rapidly during the preliminary phase of the contact period, but was delayed as the system gradually reached equilibrium. The initial rapid degradation can be attributed to the abundance of active sites on the

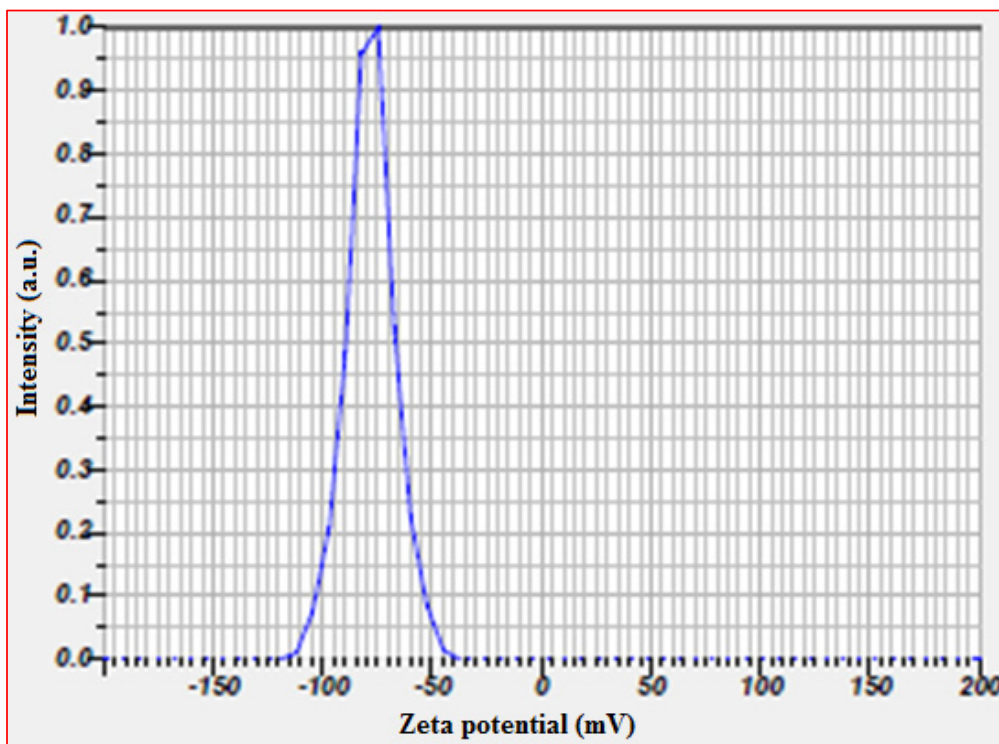


Fig. 7. Zeta potential of  $\text{Co}_3\text{V}_2\text{O}_8$ .

catalyst, but discoloration became less favored after a period of time due to the occupation of these sites. The degradation percentage, as shown in Fig. 8(b) for M.G. Dye over  $\text{Co}_3\text{V}_2\text{O}_8$  was calculated using Equation 3 and gave 89.19 [44].

$$\% \text{ Degradation} = \frac{C_o - C_e}{C_o} \times 100 \% \quad (3)$$

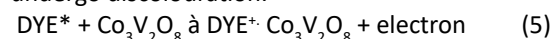
Where  $C_o$  is the initial dye concentration and  $C_e$  is the dye concentration after photodiscoloration at a time per second. Fig. 8(b) shows a plot of percent dye degradation versus irradiation time for synthesized  $\text{Co}_3\text{V}_2\text{O}_8$ . The graphs show that M.G. Dye had a higher percentage of degradation. A graph of percent degradation with time is shown in Fig. 7(c), the degradation efficiency of the synthesized sample was 89.19% for M.G.

Total organic carbon (TOC) was measured using a Shimadzu 5000 TOC analyzer to assess the mineralization of MG using the TOC method. After photodegradation, the percentage of mineralization (%TOC) of the MG dye solution was estimated using the following relationship:

$$\% \text{ TOC} = \frac{\text{TOC}_{\text{initial}} - \text{TOC}_{\text{final}}}{\text{TOC}_{\text{initial}}} \times 100 \quad (4)$$

Fig. 8(d) shows the percentage removal of total organic carbon (%TOC) [45] found in the last experiment, i.e. 60 minutes is 63% for M.G. dye solution.

Fig. 9 illustrates the mechanism of photocatalytic activity for the proposed  $\text{Co}_3\text{V}_2\text{O}_8$  dye and catalyst under UV irradiation [46, 47]. During UV Light hits  $\text{Co}_3\text{V}_2\text{O}_8$ , electrons absorb UV energy and are excited from the valence band (V.B.) into the conduction band (C.B.), resulting in an equal number of carriers, electrons and holes. The C.B. Electrons generated are transferred to the  $\text{Co}_3\text{V}_2\text{O}_8$  catalyst, which combines with ambient  $\text{O}_2$  to generate superoxide radicals. Meanwhile, as the holes in the V.B. react with the  $\text{H}_2\text{O}$ . The superoxide radicals generated during the dye activation phenomena enhance the degradation of the dye molecule [48]. The generated radicals react with the dye, break the dye molecules, and undergo discoloration.



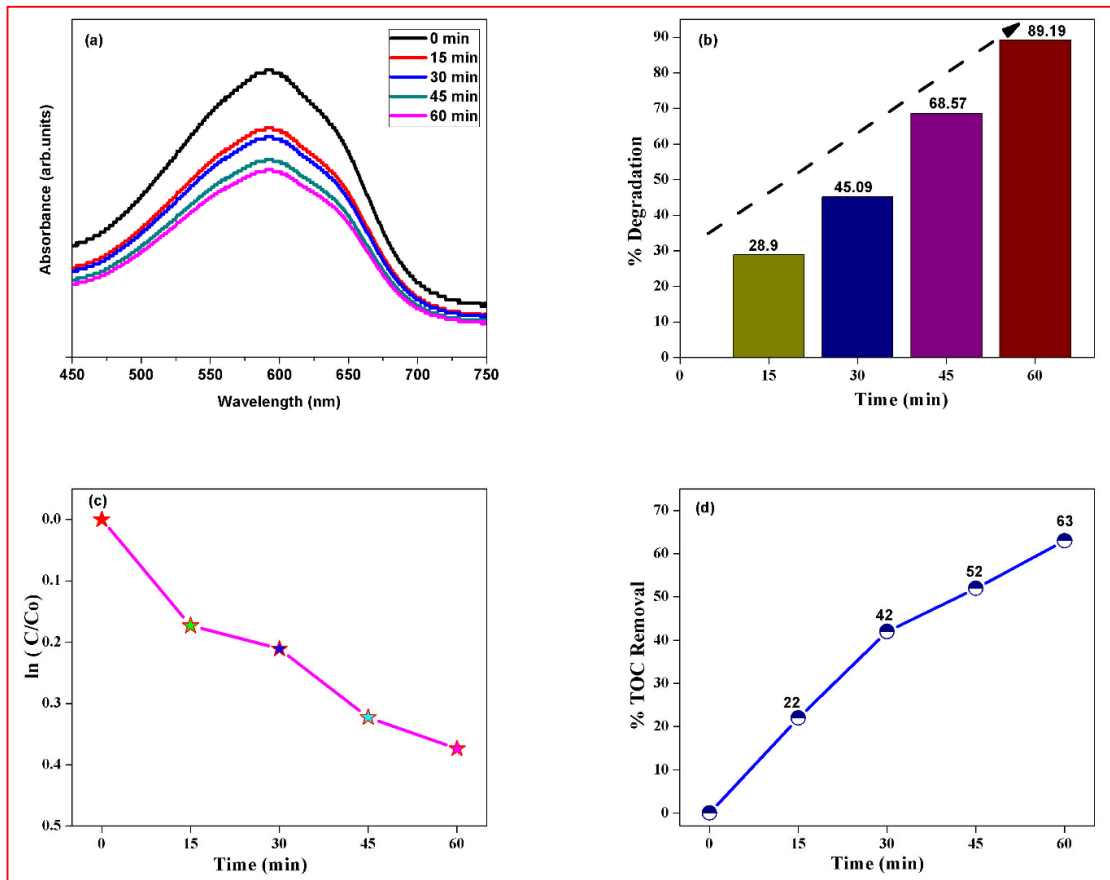


Fig. 8. (a) Absorbance spectra of M.G. (20 ppm) dye solution with  $\text{Co}_3\text{V}_2\text{O}_8$  catalyst (b) % degradation of M.G. dye solution under UV irradiation. (c) The plot of  $\ln(C/C_0)$  Vs time under UV irradiation. (d) % TOC removal plot.

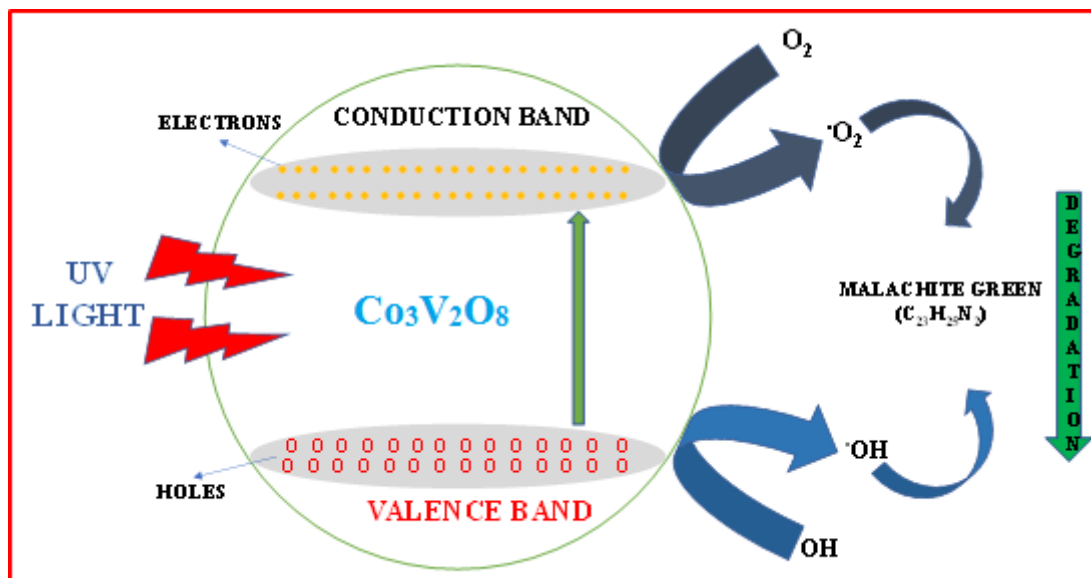
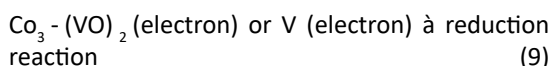
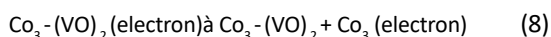


Fig. 9. Mechanism of photocatalytic activity.

Table 3. Photocatalytic degradation of Malachite Green dye by various metal oxides in aqueous solution in the literature.

Catalyst	Light source	Irradiation time (min)	Degradation (%)	Reference
10 % rGO/FeVO <sub>4</sub>	Sunlight	120	100	[49]
ZNO/CNT	Visible	60	79	[50]
Co <sub>3</sub> O <sub>4</sub>	sunlight	100	47.7	[51]
BiVO <sub>4</sub> -rGO	visible	120	99.5	[52]



The comparison of the photocatalytic degradation studies of different metal oxide nanocomposites using different light sources is given in Table 3.

### CONCLUSIONS

Co<sub>3</sub>V<sub>2</sub>O<sub>8</sub> nanostructures were fabricated using an inexpensive, simple hydrothermal process, followed by studies of extensive structural properties. The PXRD and TEM studies confirmed the material's crystal purity, finding the d-spacing for the (220) plane to be 26.6 nm with an orthorhombic structure. The studies were extended to photocatalytic properties. For the Co<sub>3</sub>V<sub>2</sub>O<sub>8</sub> sample, the energy band gap was 3.896 eV, which is sufficient to activate the materials for degradation studies when exposed to ultraviolet (UV) light. This is a good result as the breakdown of M.G. at 60 minutes was found to be 89.19%. In summary, the prepared nanospheres show enhanced photocatalytic activity in degrading M.G. bright under UV irradiation. This indicates that this nanostructure is inexpensive, highly durable and has better photocatalytic activity towards organic dye removal from wastewater/water treatment applications.

### AUTHOR CONTRIBUTION

Lakshmana Naik R conceived, designed, and conducted the study, performed the literature search, and drafted the manuscript. Balanarsaiah T was involved in the analysis, interpretation of data and reviewing. P.Justin was involved in the analysis and reviewing. All authors read and approved the final manuscript.

### CONFLICTS OF INTEREST

The authors do not have any conflicts of interest.

### REFERENCES

- [1] Kanwar V. S., Sharma A., Srivastav A. L., Rani L., (2020), Phytoremediation of toxic metals present in soil and water environment: A critical review. *Environm. Sci. Pollut. Res.* 27: 44835-44860.
- [2] Verma M., Mitan M., Kim H., Vaya D., (2021), Efficient photocatalytic degradation of Malachite green dye using facilely synthesized cobalt oxide nanomaterials using citric acid and oleic acid. *J. Phys. Chem. Solids.* 155: 110125-110129.
- [3] Lima D. R., Klein, L., Dotto, G. L., (2017), Application of ultrasound modified corn straw as adsorbent for malachite green removal from synthetic and real effluents. *Environm. Sci. Pollut. Res.* 24: 21484-21495.
- [4] Naik R. L., Narsaiah T. B., (2022), Hydrothermal synthesis and characterization of nanocrystalline zinc vanadate (Zn<sub>2</sub>V<sub>2</sub>O<sub>7</sub>) on graphene oxide scaffolds. *Materials Today: Proceed.* In Press.
- [5] Oplatowska-Stachowiak M., Elliott C. T., (2017), Food colors: Existing and emerging food safety concerns. *Crit. Rev. Food Sci. Nutr.* 57: 524-548.
- [6] Sang D. K., Wang H., Guo Z., Xie N., Zhang H., (2019), Recent developments in stability and passivation techniques of phosphorene toward next-generation device applications. *Adv. Func. Mater.* 29: 1903419.
- [7] Tong H., Ouyang S., Bi Y., Umezawa N., Oshikiri M., Ye J., (2012), Nano-photocatalytic materials: Possibilities and challenges. *Adv. Mater.* 24: 229-251.
- [8] Naciri Y., Hsini A., Ajmal Z., Navío J. A., Bakiz B., Albourine A., Benlhachemi A., (2020), Recent progress on the enhancement of photocatalytic properties of BiP<sub>04</sub> using π-conjugated materials. *Adv. Colloid and Interf. Sci.* 280: 102160.
- [9] Chen X., Mao S. S., (2007), Titanium dioxide nanomaterials: Synthesis, properties, modifications, and applications. *Chem. Rev.* 107: 2891-2959.
- [10] Maduraiveeran G., Sasidharan M., Jin W., (2019), Earth-abundant transition metal and metal oxide nanomaterials: Synthesis and electrochemical applications. *Prog. Mater. Sci.* 106: 100574.
- [11] Kayani A. B. A., Kuriakose S., Monshipouri M., Khalid F. A., Walia S., Sriram S., Bhaskaran M., (2021), UV photochromism in transition metal oxides and hybrid materials. *Small.* 17: 2100621.
- [12] Kalantar-zadeh K., Ou J. Z., Daeneke T., Mitchell A., Sasaki T., Fuhrer M. S., (2016), Two dimensional and layered transition metal oxides. *Appl. Mater. Today.* 5: 73-89.
- [13] Azadmanjiri J., Kumar P., Srivastava V. K., Sofer Z., (2020), Surface functionalization of 2D transition metal oxides and dichalcogenides via covalent and non-covalent bonding for sustainable energy and biomedical applications. *ACS Appl. Nano Mater.* 3: 3116-3143.



- [14] Monga D., Sharma S., Shetti N. P., Basu S., Reddy K. R., Aminabhavi T. M., (2021), Advances in transition metal dichalcogenide-based two-dimensional nanomaterials. *Mater. Today Chem.* 19: 100399.
- [15] Naik R. L., Justin P., Narsaiah T. B., (2020), Controllable synthesis of cobalt vanadate nanostructure materials for direct methanol fuel cell applications. *In Proceed. Int. Conf. Adv. Chem. Eng. (AdChE)*. 3728686.
- [16] Ramavathu L. N., Harapanahalli S. R., Pernapati N., Tumma B. N., (2021), Synthesis and characterization of Nickel Metavanadate ( $\text{Ni}_3\text{V}_2\text{O}_8$ )-application as photocatalyst and supercapacitor. *Int. J. Nano Dimens.* 12: 411-421.
- [17] Keerthana S. P., Yuvakkumar R., Kumar P. S., Ravi G., Velauthapillai D., (2022), Surfactant induced copper vanadate ( $\beta\text{-C}_{u2V2O7}$ ,  $\text{C}_{u3V2O8}$ ) for different textile dyes degradation. *Environm. Res.* 112964.
- [18] Ramavathu L. N., Maniam K. K., Gopalram K., Chetty R., (2012), Effect of pyrolysis temperature on cobalt phthalocyanine supported on carbon nanotubes for oxygen reduction reaction. *J. Appl. Electrochem.* 42: 945-951.
- [19] Lakshmana Naik R., Bala Narsaiah T., Ravikumar C. R., Naveen Kumar A., Vinutha K., Jahagirdar A. A., Ananda Murthy H. C., (2021), Synthesis and characterization of nickel cobalt vanadate ( $\text{NiCo}_2\text{V}_2\text{O}_8$ ) nanostructures: Photocatalytic and supercapacitor applications. *Asian J. Chem.* 33: 2831-2838.
- [20] Lakshmana Naik R., Justin P., Narsaiah B., (2020), Size controlled hydrothermal synthesis and characterization of Nickel Metavanadate ( $\text{NiVO}_3$ ) nanoparticles. *Int. J. Adv. Sci. Technol.* 29: 10012 – 10018.
- [21] Naveen Kumar Reddy K., Lakshmana Naik R., Narsaiah Tumma B., (2021), Modelling and simulation of advanced Alkaline Water electrolysis. *Int. Adv. Res. J. Sci. Eng. Technol.* 8: 729-734.
- [22] Bouchareb R., Bilici Z., Dizge N., (2021), Potato processing wastewater treatment using a combined process of chemical coagulation and membrane filtration. *Clean Soil, Air, Water.* 49: 2100017.
- [23] Zhao C., Zhou J., Yan Y., Yang L., Xing G., Li H., Zheng H., (2021), Application of coagulation/flocculation in oily wastewater treatment: A review. *Sci. Total Environm.* 765: 142795.
- [24] Gisbertz S., Pieber B., (2020), Heterogeneous photocatalysis in organic synthesis. *Chem. Photo. Chem.* 4: 456-475.
- [25] Iervolino G., Zammit I., Vaiano V., Rizzo L., (2019), Limitations and prospects for wastewater treatment by UV and visible-light-active heterogeneous photocatalysis: A critical review. *Top Current Chem.* 387: 31840195.
- [26] Ray P. C., (2010), Size and shape dependent second order nonlinear optical properties of nanomaterials and their application in biological and chemical sensing. *Chem. Rev.* 110: 5332-5365.
- [27] Hashim A., Hadi Q., (2018), Structural, electrical and optical properties of (biopolymer blend/titanium carbide) nanocomposites for low cost humidity sensors. *J. Mater. Sci: Mater. Electron.* 29: 11598-11604.
- [28] Pokhrel S., Madler L., (2020), Flame-made particles for sensors, catalysis, and energy storage applications. *Energy Fuels.* 34: 13209-13224.
- [29] Budnyak T. M., Slabon A., Sipponen M. H., (2020), Lignin-inorganic interfaces: Chemistry and applications from adsorbents to catalysts and energy storage materials. *Chem. Sus. Chem.* 13: 4344-4355.
- [30] Hakimyfarid A., Khademinia S., (2022), Hirshfeld surface analysis of solid-state synthesized  $\text{NiFe}_2\text{O}_4$  nanocomposite and application of it for photocatalytic degradation of Water pollutant dye. *Int. J. Nano Dimens.* 13: 155-167.
- [31] Nandi D., Mohan V. B., Bhowmick A. K., Bhattacharyya D., (2020), Metal/metal oxide decorated graphene synthesis and application as supercapacitor: A review. *J. Mater. Sci.* 55: 6375-6400.
- [32] Tareen A. K., Priyanga G. S., Behara S., Thomas T., Yang M., (2019), Mixed ternary transition metal nitrides: A comprehensive review of synthesis, electronic structure, and properties of engineering relevance. *Prog. Solid State Chem.* 53: 1-26.
- [33] Verma M., Mitran M., Kim H., Vaya D., (2021), Efficient photocatalytic degradation of Malachite green dye using facilely synthesized cobalt oxide nanomaterials using citric acid and oleic acid. *J. Phys. Chem. Solids.* 155: 110125.
- [34] Yang J., Wu M., Gong F., Feng T., Chen C., Liao J., (2017), Facile and controllable synthesis of solid  $\text{Co}_3\text{V}_2\text{O}_8$  micro-pencils as a highly efficient anode for Li-ion batteries. *RSC Adv.* 7: 24418-24424.
- [35] Amulya M. S., Nagaswarupa H. P., Kumar M. A., Ravikumar C. R., Prashantha S. C., Kusuma K. B., (2020), Sonochemical synthesis of  $\text{NiFe}_2\text{O}_4$  nanoparticles: Characterization and their photocatalytic and electrochemical applications. *Appl. Surf. Sci. Adv.* 1: 100023.
- [36] O'Dwyer C., Gannon G., McNulty D., Buckley D. N., Thompson D., (2012), Accommodating curvature in a highly ordered functionalized metal oxide nanofiber: Synthesis, characterization, and multiscale modeling of layered nanosheets. *Chem Mater.* 24: 3981-3992.
- [37] Aydoghmish S. M., Hassanzadeh-Tabrizi S. A., Saffar-Teluri A., (2019), Facile synthesis and investigation of NiO-ZnO-Ag nanocomposites as efficient photocatalysts for degradation of methylene blue dye. *Ceram. Int.* 45: 14934-14942.
- [38] Xiao M., Yang D., Yan Y., Tian Y., Zhou M., Hao M., Miao Y., (2015), Nanoplates and nanospheres of  $\text{Co}_3(\text{VO}_4)_2$  as noble metal-free electrocatalysts for oxygen evolution. *Electrochim. Acta.* 180: 260-267.
- [39] Xing M., Kong L. B., Liu M. C., Liu L. Y., Kang L., Luo Y. C., (2014), Cobalt vanadate as highly active, stable, noble metal-free oxygen evolution electrocatalyst. *J. Mater. Chem. A.* 2: 18435-18443.
- [40] Hu L., Shang C., (2020),  $\text{Co}_3\text{V}_2\text{O}_8$  nanoparticles supported on reduced graphene oxide for efficient lithium storage. *Nanomater.* 10: 740-746.
- [41] Youn C., Shin S., Shin K., Kim C., Park C. L., Choi J., Kim S. H., Yeo S. Y., Shin M. W., Henkelman G., Yoon K. R., (2022), Template-assisted synthesis of single-atom catalysts supported on highly crystalline vanadium pentoxide for stable oxygen evolution. *Chem. Catalysis.* 2: 1-20.
- [42] Ijaz F., Shahid S., Khan S. A., Ahmad W., Zaman S., (2017), Green synthesis of copper oxide nanoparticles using a butilon indicum leaf extract: Antimicrobial, antioxidant and photocatalytic dye degradation activities. *Tropical J. Pharmac. Res.* 16: 743-753.
- [43] Mafa P. J., Malefane M. E., Idris A. O., Mamba B. B., Liu D., Gui J., Kuvarega A. T., (2021), Cobalt oxide/copper bismuth oxide/samarium vanadate ( $\text{Co}_3\text{O}_4/\text{CuBi}_2\text{O}_4/\text{SmVO}_4$ ) dual Z-scheme heterostructures photocatalyst with high



- charge-transfer efficiency: Enhanced carbamazepine degradation under visible light irradiation. *J. Colloid Interf. Sci.* 603: 666-684.
- [44] Faniband S. M., Vidyasagar C. C., Jimenez V., Shridhar A. H., (2022), Mechanistic insight into the photocatalytic degradation of organic pollutant and electrochemical behavior of modified MWCNTs/Cu-Co<sub>3</sub>O<sub>4</sub> nanocomposite. *React. Chem. Eng.* 7: 1847-1872.
- [45] Parsa M. M., Pourfakhar H., Baghdadi M., (2020), Application of graphene oxide nanosheets in the coagulation-flocculation process for removal of Total Organic Carbon (TOC) from surface water. *J. Water Proc. Eng.* 37: 101367.
- [46] Azari B., Pourahmad A., Sadeghi B., Mokhtary M., (2019), Preparation and photocatalytic study of SiO<sub>2</sub>/CuS coreshell nanomaterial for degradation of methylene blue dye. *Nanoscale.* 6: 103-114.
- [47] Zhao Y., Liu Y., Du X., Han R., Ding Y., (2014), Hexagonal assembly of Co<sub>3</sub>V<sub>2</sub>O<sub>8</sub> nanoparticles acting as an efficient catalyst for visible light-driven water oxidation. *J. Mater. Chem. A.* 2: 19308-19314.
- [48] Zhang H., Guan W., Zhang L., Guan X., Wang S., (2020), Degradation of an organic dye by bisulfite catalytically activated with iron manganese oxides: The role of superoxide radicals. *ACS Omega.* 5: 18007-18012.
- [49] Alsulami Q. A., Rajeh A., Mannaa M. A., Albukhari S. M., Baamer D. F., (2021), Preparation of highly efficient sunlight driven photodegradation of some organic pollutants and H<sub>2</sub> evolution over rGO/FeVO<sub>4</sub> nanocomposites. *Int. J. Hydrogen Energy.* 46: 27349–27363.
- [50] Arsalani N., Bazazi S., Abuali M., Jodeyri S., (2019), A new method for preparing ZnO/CNT nanocomposites with enhanced photocatalytic degradation of malachite green under visible light. *J. Photochem. Photobiol. A: Chem.* 389: 112207.
- [51] Verma M., Mitan M., Kim H., Vaya D., (2021), Efficient photocatalytic degradation of Malachite green dye using facilely synthesized cobalt oxide nanomaterials using citric acid and oleic acid. *J. Phys. Chem. Solids.* 155: 110125.
- [52] Zhang M., Gong J., Zeng G., Zhang P., Song B., Cao W., Huan S., (2018), Enhanced degradation performance of organic dyes removal by bismuth vanadate-reduced graphene oxide composites under visible light radiation. *Colloids Surf. A: Physicochem. Eng. Asp.* 559: 169-183.

